SCIENTIFIC REPORTS

OPEN

SUBJECT AREAS:

MECHANICAL PROPERTIES

CHARACTERIZATION AND ANALYTICAL TECHNIQUES

Received
24 July 2013

Accepted
1 August 2013

Published
30 August 2013

Correspondence and requests for materials should be addressed to H.V.S. (helena.vanswygenhoven@psi.ch)

{110} Slip with {112} slip traces in bcc Tungsten

Cecile Marichal[1,2], Helena Van Swygenhoven[1,2], Steven Van Petegem[1] & Camelia Borca[3]

[1]Materials Science and Simulation, NUM/ASQ, Paul Scherrer Institut, CH-5232 Villigen PSI, Switzerland, [2]Neutrons and X-rays for Mechanics of Materials, IMX, École Polytechnique Fédérale de Lausanne, CH-1012 Lausanne, Switzerland, [3]Beamline MicroXAS, Paul Scherrer Institut, CH-5232 Villigen PSI, Switzerland.

While propagation of dislocations in body centered cubic metals at low temperature is understood in terms of elementary steps on {110} planes, slip traces correspond often with other crystallographic or non-crystallographic planes. In the past, characterization of slip was limited to post-mortem electron microscopy and slip trace analysis on the sample surface. Here with in-situ Laue diffraction experiments during micro-compression we demonstrate that when two {110} planes containing the same slip direction experience the same resolved shear stress, sharp slip traces are observed on a {112} plane. When however the {110} planes are slightly differently stressed, macroscopic strain is measured on the individual planes and collective cross-slip is used to fulfill mechanical boundary conditions, resulting in a zig-zag or broad slip trace on the sample surface. We anticipate that such dynamics can occur in polycrystalline metals due to local inhomogeneous stress distributions and can cause unusual slip transfer among grains.

Dislocations are line defects in a crystal characterized by their slip plane, their Burgers vector and the orientation of the Burgers vector relative to the dislocation line. In metals with a face centered crystal lattice (fcc) the strain field of dislocations is confined in a {111} plane and the resistance to glide, the Peierls-Nabarro resistance[1,2], is small. Dislocation response to stress is easy predictable and usually controlled by the resolved shear stress on the slip plane as described by Schmid's law[3]. That is why computational models for fcc plasticity experienced enormous progress in the last decennia.

The body-centered cubic crystal lattice (bcc) has no real closed packed planes and the strain field of screw dislocations is non-planar[4]. Dislocation slip depends on the loading axis and the sense of shearing in the crystallographic plane. The nature of this anisotropy is still under debate. Slip has been reported in pure metals on {110} and {112} planes[5–8]. Many particular aspects of the deformation characteristics in bcc metals are ascribed to the 3-dimensional core structure of screw dislocations, which is consequently anchored in the lattice[9,10]. Most of the details on the core structure of screw and on the slip mechanisms are obtained from atomistic simulations[4,11–15] revealing aspects such as the role of stresses other than the resolved shear stress that break the symmetry of the core structure[16] or the role of other particular orientations corresponding with a high Peierls stress[17]. These new aspects form important input for higher-lengthscale models such as discrete dislocation simulation models used to investigate the yield and plastic behavior of a bcc single crystal[17–22]. So far, these computational efforts have provided much more details than what currently has been validated experimentally, but the extrapolation towards larger lengthscales remains difficult because of a lack in understanding of the full dynamic picture of dislocation plasticity.

It is now generally believed that a screw dislocation moves in the lattice potential by thermal activated nucleation of a pair of kinks in {110} crystal planes[23], bringing a segment of the dislocation over the potential hill of the lattice. The kinks can rapidly propagate in the <111> direction along the dislocation line advancing the whole dislocation to the next equilibrium Peierls valley[9,10]. An open questions is whether a {112} slip trace on the surface of a crystal results from a composition of slip on several{110} planes.

For instance, consider uniaxial compression performed at room temperature along a crystallographic direction [155]. Figure 1a shows the compression axis in stereographic projection together with some crystallographic directions and the projections of the normal of crystallographic planes of interest. In this orientation, the Schmid factor m, which relates the resolved shear stress for a particular slip system to the applied stress, equals its maximal value of 0.5 for slip on the (211) plane in the [1-1-1] direction, meaning that the resolved shear stress is highest on the (211) plane. The (101) and (110) planes are the planes of the {110} family that have the highest Schmid values, for both $m = 0.43$, in the same [1-1-1] direction. Assuming that elementary slip occurs on {110} planes, screw dislocations will propagate in this loading direction with equal amounts of elementary steps on the (101) and

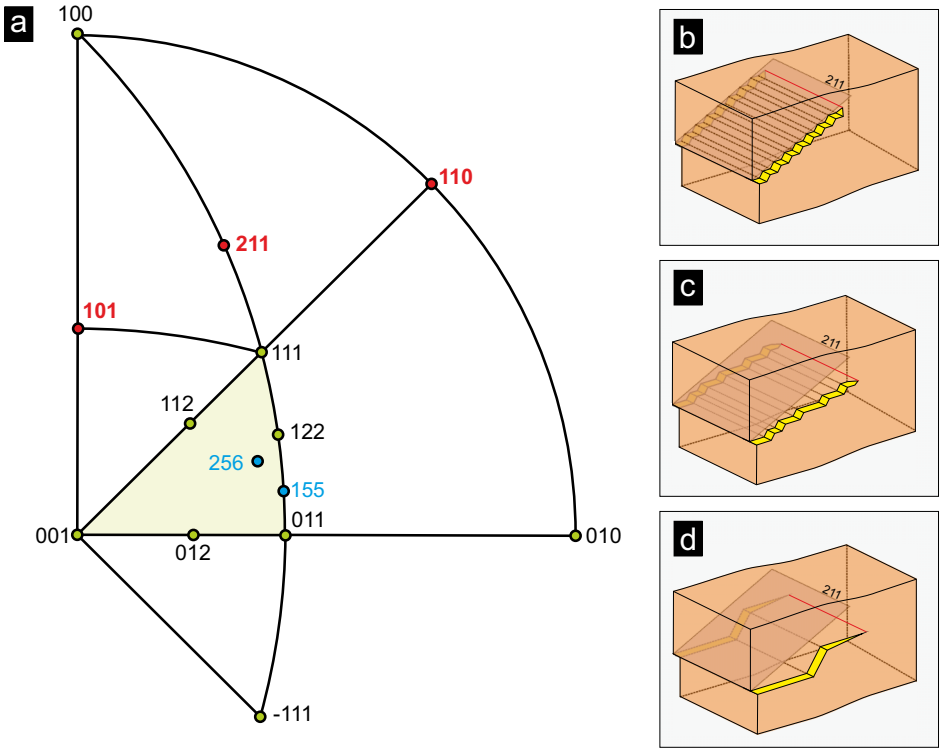

Figure 1 | Presentation of the [155] and [256] compression axis in stereographic projection (a); schematic presentation of elementary slip steps on (110) and (101) in equal portions (b), in elementary steps proportional to the resolved shear stress (c) and producing macroscopic slip on the individual (110) and (101) planes (d).

(110) plane, as is schematically presented in Figure 1b. When reaching the surface of the sample, the slip trace would be composed of elementary {110} steps that are experimentally however not observable. What can be measured is the averaged orientation of the slip trace, which corresponds in this orientation with the (211) plane[6,7,24].

For an orientation of the compression axis slightly different such as [256], keeping the Schmid factor highest ($m = 0.49$) for the (211) plane but slightly different for the (101) and (110), respectively $m = 0.45$ and $m = 0.39$, one assumes elementary steps on each plane occurring proportional to the ratio of the Schmid factors, as schematically presented in Figure 1c. This is the common philosophy behind the interpretation of slip traces observed on the surface of single crystals but there are no experiments reported in these orientations confirming the above concept behind the interpretation of slip traces. In the past, experiments were mainly limited to surface slip trace analysis and post-mortem transmission electron microscopy (TEM). Today's advanced in-situ techniques can however go further.

Here we use micro-compression testing during in-situ Laue diffraction performed on single crystal tungsten (W) pillars in different crystallographic orientations. Since Tc equals 527°C in tungsten[25], experiments performed at room temperature are far below the critical temperature. For details on the setup we refer to Methods section. Laue diffraction is very sensitive to changes in orientation of the crystal planes[26–29]. During micro-compression experiments, the single crystal pillar is constrained during the load. Consequently, the planes where the dislocations are moving are rotating to accommodate the stress[21]. During elastic loading, minor rotation can be observed due to distortion of the unit cell. During plastic deformation, using the Taylor model, the observed rotation can be assigned to the activated plane(s) by considering the rotation axis as the cross product between the compression axis and the normal of the slip plane. In other words, the path followed by the Laue spots during deformation provides information on the activated slip system.

Results

Compression along the [155] axis confirms that slip can be described with elementary steps on {110} planes. Figure 2a provides the stress-strain curve obtained from a pillar with a diameter of 1.9 μm. The numbers figuring on the plot correspond with snapshots of Laue diffraction patterns taken continuously during the load. The scatter on the stress-strain curve is due to the open-air working conditions, which is required for operating in-situ.

Figure 2b shows the (-3-10) Laue reflection before deformation. The projected lines correspond with the expected rotation directions for slip on particular crystallographic planes. Figure 2c shows the path followed by the center of mass of the (-3-10) reflection in detector units during compression; the numbers correspond with those shown on the stress-strain curve in Figure 2a. During the elastic loading the peak moves away from its initial position. This rotation is caused by elastic distortion of the crystal and accommodation between the pillar top and the compression anvil. Load-unload experiments formerly carried out on pillars with similar diameter demonstrated that after unloading peak broadening and position recover entirely when the load in these pillars did not exceed 600 MPa (pattern 30). Taking into account all other reflections and using the Taylor model, the movement of the Laue spots corresponds with a rotation of 0.50 degree around the [211] direction. Upon further rotation, the path of the Laue spot stays clearly parallel to the rotation direction for slip on the (211) plane which also corresponds with that for composed slip on (101) and (110). This path is rather smooth and up to pattern 40 no individual jumps are observed. Between pattern 40 and 58 some of the steps can be also assigned to an excess of slip on one of the {110} planes. After pattern 58, which corresponds with the major bursts in the stress-strain curve, the (211) rotation direction is followed again. Figure 2d shows the scanning electron microscopy (SEM) image of the pillar after deformation, evidencing a well-defined slip trace corresponding with the (211) plane schematically presented in red.

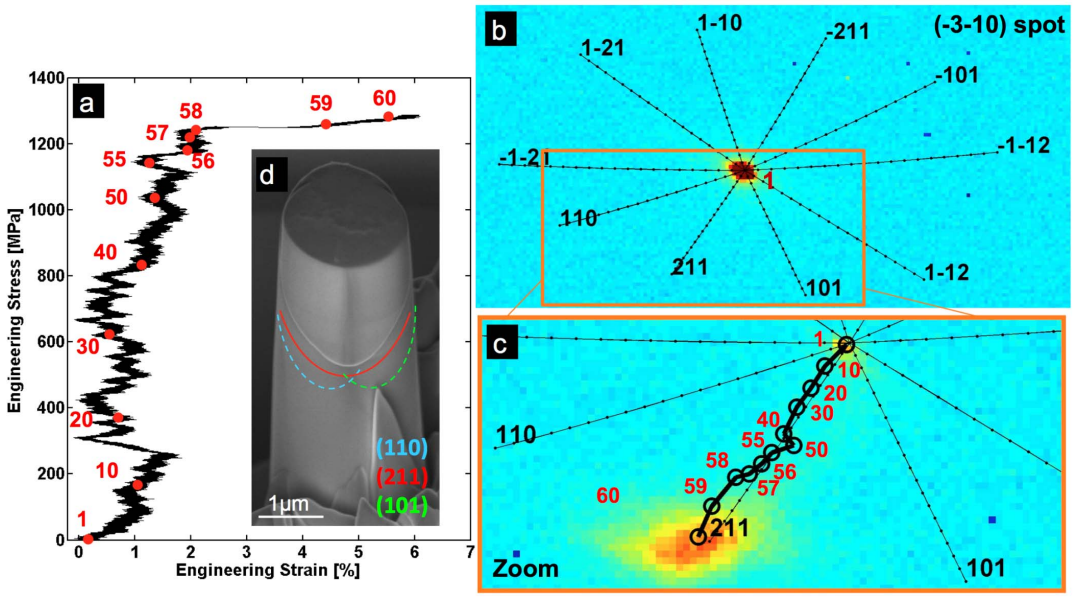

Figure 2 | In-situ results of W single crystal with [155] compression axis. (a) Stress-strain curve (b) Two dimensional representation of the (-3-10) diffraction spot plotted together with the lines corresponding to rotation directions for slip on particular planes. (c) Zoom-in and path followed by the (-3-10) spot during the compression, the numbers correspond to the stress stages in (a); (d) Slip trace visible on a SEM picture taken after deformation corresponding with (211) plane indicated in red. The green and blue lines correspond with (110) and (101) plane orientation on which no traces are observed.

So far the Laue results confirm that in the athermal regime slip can be described as composed of elementary steps on {110} planes. This is however not the case in orientations for which the Schmid factors on the most stressed {110] planes differ slightly. The character of slip changes drastically when a [256] oriented pillar is compressed. Figure 3a shows the stress-strain curve of such a pillar, Figure 3b the (101) Laue reflection as well as the possible rotation directions plotted with white lines. A zoom-in of the orange square is shown on Figure 3c, where the path followed by the (101) spot during loading is presented by the yellow line. The numbers along the Laue path correspond with the numbers shown on the stress-strain curve. During initial loading till 650 MPa (corresponding with pattern 35), the (101) Laue peak moves slightly in a direction that does not correspond with any crystallographic slip.

Taking into account all other reflections and using the Taylor model, the movement of the Laue spots corresponds with a rotation of 0.75 degree around an axis in between the [110] and the [211] direction. Such a small rotation does not change the values of the Schmid factors (only the third decimal). Loading till 900 MPa (pattern 45) causes the Laue spot to follow the line for rotation according to slip on the (110) plane. From pattern 45 to 48, the path of the Laue spot changes direction suggesting equal slip on the (110) and (101) plane resulting in a rotation along the (211) line. Upon further loading the (101) spot jumps discontinuously and some of the directions

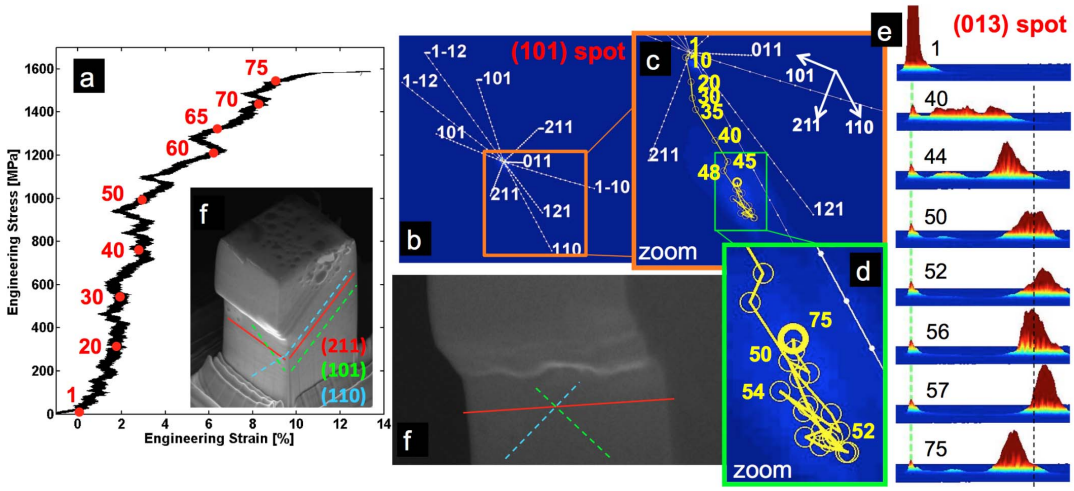

Figure 3 | In-situ results of a W single crystal with [256] compression axis. (a) Stress-strain curve (b) Two dimensional representation of the (101) diffraction spot. The white lines present the expected rotation direction for slip on the indicated planes. (c) Zoom-in on the path followed by the (101) spot during the compression, the pattern numbers correspond to the stress values shown in (a). (d) Zoom-in of the very jerky part of the spot path surrounded in green on (c). (e) this back and forward movement of the peak along the rotation direction for (101) and (110) slip is shown in more detail for the (013) diffraction spot and with a different viewing angle. (f) Two views of the slip trace visible on SEM pictures taken after deformation.

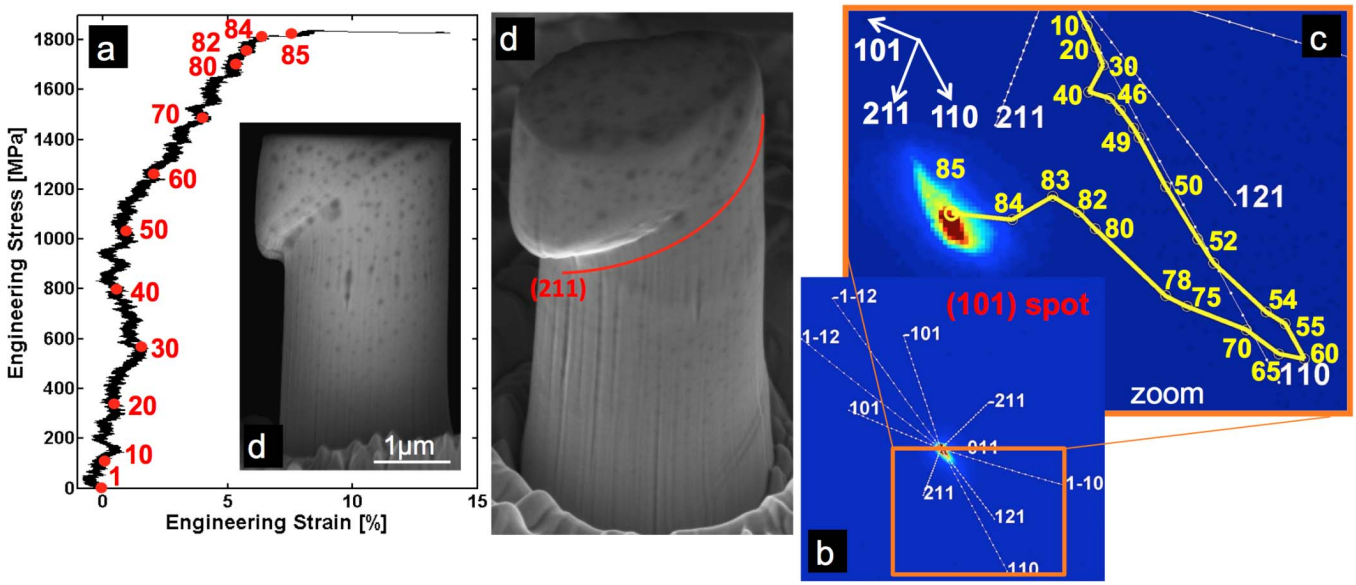

Figure 4 | In-situ result of a second W micro-pillar with a compression axis along [256]. (a) Stress-strain curve (b) Two dimensional representation of the (101) diffraction spot. The white lines present the expected rotation direction for slip on the indicated planes. (c) Zoom-in on the path followed by the (101) spot during the compression, the numbers correspond to the stress values shown in (a); (d) Two views on the slip trace visible on SEM pictures taken after deformation.

correspond with slip on (110) others with slip on (101) as for instance the strain produced between pattern 52 and pattern 54. The latter can be viewed in more detail in the further zoom-in region of Figure 3d (green frame). This back and forward movement of the peak along the rotation direction for (101) and (110) slip is shown in more detail in Figure 3e for the (013) Laue reflection. Here the viewing angle is perpendicular to the rotation direction for slip on (110). At the end of the loading path a moderate burst is recorded at 1550 MPa, which corresponds in the Laue patterns with a rotation for slip on (110). The SEM pictures in Figure 3f show a broad unsharp slip trace with an envelope that corresponds with a (211) plane. The amount of strain accommodated by the slip trace is higher than the strain produced in the strain burst. When zooming in on the slip trace, it is clear that this broad trace consists of several smaller traces which together form wavy substructures. The direction of the substructures reflects slip traces produced by the (101) and (110) slip planes as suggested by the colored lines on the SEM picture. In other words, slip trace and the Laue analysis demonstrate slip to occur on the two (110) planes with highest Schmid factor, however macroscopic strain is produced on the individual slip planes. The important jumps of the Laue reflections together with the zig-zag slip trace suggest collective cross-slip used as mechanism to fulfill the mechanical boundary conditions imposed by compression along [256].

Among the pillars studied, other combinations of collective cross-slip have been observed. Figure 4a shows the stress-strain curve of another [256] oriented pillar together with numbers of corresponding Laue patterns. The path of the (101) diffraction spot is shown in Figure 4b together with a projection of the possible rotation directions. The region of interest is zoomed in Figure 4c. Till pattern 32 corresponding with 600 MPa Laue spots broaden and simultaneously rotate about 0.36° degree this time in the direction corresponding to slip in the (110) plane. Between pattern 30 and 40 there is a discontinuous change of rotation direction indicating a rotation corresponding with (211) i.e. resulting from composed slip on the (110) and (101) planes. Between pattern 40 and 60 the Laue peak moves predominantly according to slip on (110) after which the spot clearly changes direction and rotates predominantly according to slip on (101), suggesting collective cross-slip. At pattern 83 until the end of the load, the peak changes again and follows a direction suggesting combined slip on (110) and (101). Note that at pattern 85, the global rotation evidenced by Laue corresponds to a rotation along the (211) line.

The load sequence ends with an important strain burst appearing at 1800 MPa during which only a minor additional rotation along the (211) line is observed. Inspection of the surface of the sample after deformation revealed one very broad slip trace corresponding with a (211) plane, visible on Figure 4d. In this case, no substructure can be observed.

It needs to be remarked that the differences in flow stress between the discussed pillars at a same strain value can be assigned to the differences in size (for details see Table 1), a phenomenon that is well known[30] but no matter of interest in this paper.

Discussion

The Laue diffraction experiments on W at room temperature show that dislocation slip occurs on {110} planes. This is in line with the double kink model for the propagation of screw dislocations in the bcc lattice in the athermal regime (i.e. below the critical temperature). In an orientation where two {110} planes have the same resolved shear stress, slip can be described by alternating elementary steps on both planes so that the overall rotation is similar to effective slip on (211). This is also reflected in the (211) slip trace on the sample surface. The situation is however different when the resolved shear stress on the {110} planes is non-equal. Our experiments demonstrate that slip does not occur anymore by frequent alternation of elementary steps proportional to the resolved shear stress of the two most stressed {110} planes. Instead dislocations can propagate on one of the highly stressed {110} planes, produce macroscopic strain and cross-slip collectively as schematically represented in Figure 1d. Collective cross-slip is the mechanism that allows fulfilling the mechanical boundary conditions here represented by a highest resolved shear stress on the (211) plane. The slip trace corresponds to the plane expected according to the mechanical boundary conditions, loses however its sharpness revealing eventual substructures that reflect the individual slip systems.

In a micro-compression experiment the single crystal sample usually experiences an inhomogeneous stress distribution. This is also the case in our experiments. During elastic compression, the Laue

Orientation	Shape	Width (μm) Cross-section (μm²) Height (μm)	Schmid Factors			SEM images
			(211)[1-1-1]	(101)[1-1-1]	(110)[1-1-1]	
[155]	Round	1.9 2.9 6.5	0.50	0.44	0.43	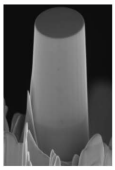
[256]	Square	2.1 4.7 5.1	0.49	0.45	0.39	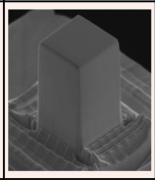
[256]	Round	1.8 2.5 5.5	0.49	0.45	0.39	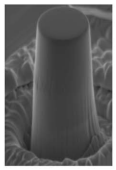

Figure 5 | Overview of the properties of the tungsten pillars under investigation, including pillar geometry and Schmid factors of relevant slip systems. The last column provides SEM images of the pillars prior to deformation.

peaks do not always rotate along the predicted direction for the particular reflection but often rotate in a non-crystallographic direction. This rotation is minor and in most cases less then 0.75° so that it has no major influence on the ratio of the resolved shear stresses. It is however an indication for local inhomogeneous stresses as was already reported earlier[31]. The role played by these inhomogeneous stresses in bcc metals is observed to have much more important consequences than in fcc single crystals. Misalignments up to 2° induce initial slip activity of geometrically less favorable slip systems in fcc pillars[31] but already after 1 to 2% macroscopic strain slip is taken over fully as expected and predicted by Schmid rules. In bcc crystals this is also the case for the [155] orientation where the two {110} planes are equally stressed however in the [256] orientation the small difference in resolved shear stress combined with the presence of heterogeneous stress distribution disturbs the mechanism of composed slip. Instead of progressing with elementary steps using frequent cross-slip, slip continues on the chosen {110} plane and produces macroscopic strain. Our experiments suggest that strain is produced on this system as long as mechanical compatibility requirements allow, after which collective cross-slip operates and slip on the secondary {110} system provides the mechanically required crystal rotation.

What are the important consequences of these observations? Inhomogeneous stress distributions within a plastifying volume are unavoidable. In a single crystal, this can occur as a result of, for instance, boundary constraints of the experimental setup such as here in a compression experiment[31], or thermal or elastic mismatch between a thin film and its substrate[32]. In single-phase polycrystals the interplay between individual grain orientation, size and shape, and deformation properties such as elastic-plastic anisotropy and

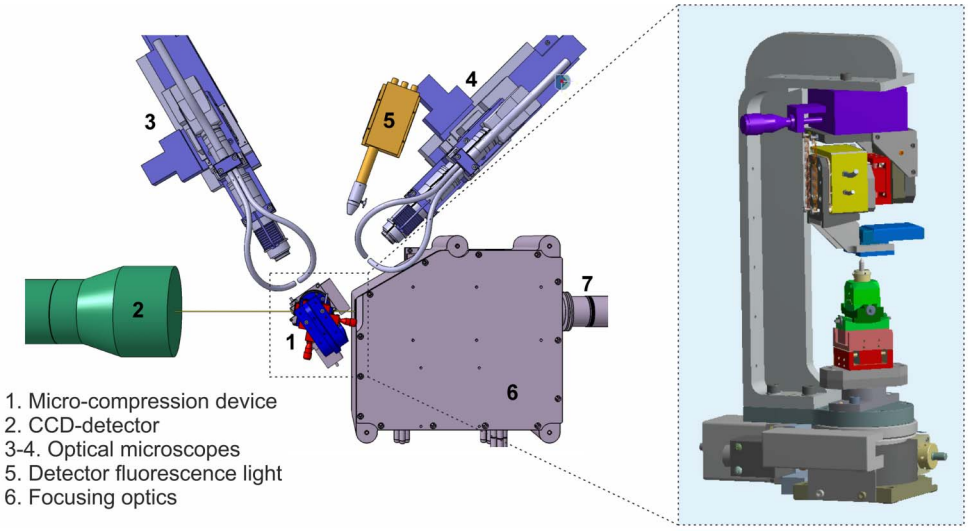

Figure 6 | Schematic view of the in situ Laue microdiffraction setup installed at the MicroXAS beam line of the Swiss Light Source. The inset displays the custom-built micro-compression device, consisting of various translation, tilting and rotation stages for alignment and a 1D Hysitron transducer to perform the actual compression experiment.

strain hardening mechanisms are known to be at the origin of the grain-to grain differences in average grain stresses. Slip incompatibilities at interfaces and triple junctions create inhomogeneous stresses and stress gradients at the subgrain scale. The role of such local stress concentrations has been recognized in deformation twinning in hexagonal close packed metals. The observed diversity in twins in similar oriented grains has triggered the development of a probabilistic twin nucleation model[33]. The role of local fluctuations in stress or stress gradients are also the focus of attention in studies on nucleation of damage or size dependent strengthening[34–36].

Our results add a previously unrevealed aspect of non uniform local stress fluctuations: they can change the character of composed slip from frequently alternating elementary steps proportional to the resolved shear stress into slip producing macroscopic strain on one particular {110} plane followed by the second system to fulfill the boundary conditions. In polycrystalline structures, this can have major impact on the transfer of strain with possible transmission of unexpected slip systems, having consequences for further plasticity and development of damage. This work advocates for future research into the influence of local stress distributions on composed slip as well as the parameterization of slip mechanism by the formulation of cross-slip rules in discrete dislocation models.

Methods

Pillars fabrication. For the Laue micro-diffraction experiments free-standing micro-pillars have been prepared. Two foils of single crystal tungsten in a [155] and [256] crystallographic orientation with initial thickness of 100 μm have been obtained from Mateck Company ensuring a 5N purity. They have both been thinned down to a final thickness of approximately 30 μm by electropolishing in an electrolyte of 250 mL of distilled water with 25 g of sodium hydroxide applying a current of 6 V. This step allows removing the thin defects layer introduced during production and to economize FIB time. Conventional high-resolution focused ion beam coupled with a scanning electron microscope has been used to fabricate the presented micro-pillars at the thin foil extremity. Ion currents in the range from 6.5 nA to 40 pA have been applied sequentially with an accelerating voltage of 30 kV. First a pillar base of $10 \times 10\ \mu m^2$ is created using a current of 6.5 nA. Then this is reduced to a base with a diameter of three times the final pillar diameter. The step milling process to create the final pillar employs very low currents down to 40 pA. The square pillars exhibit no taper whereas the round pillars have a taper angle of approximately 2°. To ensure a flat top the pillars are cut with a current of 10 pA. An overview of the properties of the tungsten pillars is provided in Figure 5. Note that the actual compressions axis are up to 0.7° off from the nominal [155] and [256] direction, as determined by x-ray Laue diffraction. The tabulated Schmid factors are therefore calculated with these corrected values.

***In situ* Laue diffraction.** In-situ Laue micro-compression experiments are performed at the MicroXAS beam line of the Swiss Light Source. Figure 6 displays a schematic view of the setup. The sample is illuminated by a polychromatic x-ray beam (5–23 keV) with a spot size of 1 μm. The diffracted beam is recorded with a 16-bit CCD-detector (Photonic Science). Sample alignment is done with the help of two high-resolution optical microscopes and an x-ray fluorescence detector.

The micropillars are compressed at a constant load rate of 5.5 μm/s by a 1D transducer (Hysitron Incorp.), which is mounted in a frame consisting of multiple translation, tilting and rotation stages. Diffraction patterns are recorded every 10 s. Indexation and peak analysis were performed with a custom-written software-package coded with Matlab. For more details we refer to[27].

1. Peierls, R. The size of a dislocation. *Proc Phys Soc* **52**, 34–43 (1940).
2. Nabarro, F. R. N. Dislocations in a simple cubic lattice. *Proc Phys Soc* **59**, 256–272 (1947).
3. Schmid, E. & Boas, W. *Kristallplastizität.*, Springer, Berlin (1935), translated in English: *Plasticity of Crystals* by F. A. Hughes & Co. (1950).
4. Vitek, V. Structure of dislocation cores in metallic materials and its impact on their plastic behavior. *Prog. Mater. Sci.* **36**, 1–27 (1992).
5. Christian, J. W. Some surprising features of the plastic deformation of Body-Centered Cubic metals and alloys. *Met. Trans. A* **14A**, 1237 (1983).
6. Spitzig, W. A. & Keh, A. S. The effect of orientation and temperature on the plastic flow properties of iron single crystals. *Acta Met.* **18**, 611 (1970).
7. Hull, D., Byron, J. F. & Noble, F. W. Orientation dependence of yield in body-centered cubic metals. *Can J Phys.* **45**, 1091–1099 (1967).
8. Seeger, A. Peierls berriers, kinks, and flow stress: recent progress. *Z. Metallkd* **93**, 760 (2002).
9. Argon, A. in *Strengthening Mechanisms in Crystal Plasticity, Oxford Series on Materials Modelling* (2008).
10. Hirth, J. P. & Lothe, J. in *Theory of dislocations,* eds Krieger (1982).
11. Groeger, R., Bailey, A. G. & Vitek, V. Multiscale modeling of plastic deformation of molybdenum and tungsten: I. Atomistic studies of the core structure and glide of ½<111> screw dislocations at 0 K. *Acta Mat.* **56**, 5401 (2008).
12. Kang, K., Bulatov, V. V. & Cai, W. Singular orientations and faceted motion of dislocations in body-centered cubic crystals. *Proc. Nat. Acad. Science* **109**, 15174–15178 (2012).
13. Weinberger, C. R., Tucker, G. J. & Foiles, S. M. Peierls potential of screw dislocations in bcc transition metals: Predictions from density functional theory. *Phys. Rev. B* **87**, 054114 (2013).
14. Cereceda, D. *et al.* Assessment of interatomic potentials for atomistic analysis of static and dynamic properties of screw dislocations in W. *J. of Phys. Cond. Mat.* **25**, 085702 (2013).
15. Woodward, C. & Rao, S. I. Ab-initio simulation of isolated screw dislocations in bcc Mo and Ta. *Phil. Mag A* **81**, 1305–1316 (2001).
16. Gröger, R., Bailey, A. G. & Vitek, V. Multiscale modeling of plastic deformation of molybdenum and tungsten: I. Atomistic studies of the core structure and glide of ½<111> screw dislocations at 0 K. *Acta Mat.* **56**, 5401–5411 (2008).
17. Kang, K., Bulatov, V. V. & Cai, W. Singular orientations and faceted motion of dislocations in body-centered cubic crystals. *Proc. Nat. Acad. Science* **109**, 15174–15178 (2012).
18. Ariza, M. P., Tellechea, E., Menguiano, A. S. & Ortiz, M. Double kink mechanisms for discrete dislocations in BCC crystals. *Int J Fract* **174**, 29–40 (2012).
19. Weinberger, C. R., Battaile, C. C., Buchheit, T. E. & Holm, E. A. Incorporating atomistic data of lattice friction into BCC crystal plasticity models. *Int. Jnl of Plasticity* **37**, 16–30 (2012).
20. Srivastava, K., Groger, R., Weygand, D. & Gumbsch, P. Dislocation motion in tungsten: atomistic input to discrete dislocation simulations. *Int J Plast.* **47**, 126 (2013).
21. Chaussidon, J., Robertson, C., Rodney, D. & Fivel, M. Dislocation dynamics simulations of plasticity in Fe laths at low temperature. *Acta Mater.* **56**, 5466–5476 (2008).
22. Li, D., Zbib, H., Sun, X. & Khaleel, M. Predicting plastic flow and irradiation hardening of iron single crystal with mechanism-based continuum dislocation dynamics. *Int. J. Plast.* In Press, Corrected Proof, Available online 4 February 2013. (2013).
23. Caillard, D. Kinetics of dislocations in oure Fe. Part I. In situ straining experiments at room temperture. *Acta Mat* **58**, 3493 (2010).
24. Han, S. M. *et al.* Critical-temperature/Peierls-stress dependent size effects in body centered cubic nanopillars. *Appl. Phys. Lett.* **102**, 041910 (2013).
25. Sestak, B. & Seeger, A. Gleitung und verfestigung in kubisch-raumzentrierten Metallen und Legierungen. *Z. Metallkde* **69**, 195–202 (1978).
26. Hosford, W. F. in *The Mechanics of Crystals and Textured Polycrystals*, eds. Oxford University Press (1993).
27. Van Swygenhoven, H. & Van Petegem, S. The use of Laue microdiffraction to study small-scale plasticity. *JOM* **62**, 36–43 (2010).
28. Barabash, R. I., Ice, G. E., Kumar, M. & Belak, J. l. Polychromatic microdiffraction analysis of defect self-organization in shock deformed single crystals. *Int J Plast* **25**, 2081–2093 (2009).
29. Larson, B. C. & Levine, L. E. Submicrometre-resolution polychromatic three-dimensional X-ray microscopy. *J. Appl Crystallogr* **46**, 153–164 (2013).
30. Uchic, M. D., Dimiduk, D. M., Florando, J. N. & Nix, W. D. Sample dimensions influence strength and crystal plasticity. *Science* **305**, 986–989 (2004).
31. Maass, R. *et al.* Smaller is stronger: the effect of strain hardening. *Acta Mat.* **57**, 5996–6005 (2009).
32. Nicola, L., Van der Giessen, E. & Needleman, A. Discrete dislocation analysis of size effects in thin films. *J. Appl. Phys.* **93**, 5920–5928 (2003).
33. Beyerlein, I. J. & Tomé, C. N. A probabilistic twin nucleation model for HCP polycrystalline metals. *Proc. R. Soc. A* **466**, 2517–2544 (2010).
34. Rollett, A. D., Lebensohn, R. A., Groeber, M., Choi, Y., Li, J. & Rohrer, G. S. Stress hot spots in viscoplastic deformation of polycrystals. *Modelling Simul. Mater. Sci. Eng.* **18**, 074005 (2010).
35. Wilkinson, A. J. & Randman, D. Determination of elastic strain fields and geometrically necessary dislocation distributions near nanoindents using electron back scatter diffraction. *Philos Mag* **90**, 1159–1177 (2010).
36. Chakrawarthy, S. S. & Curtin, W. A. Stress-gradient plasticity. *Proc. Nat. Acad. Science* **108**, 15716–15720 (2011).

Acknowledgements

Authors are grateful to S. Pierret, M. Weisser, C. Le Bourlot, A. Irastorza, S. Zabihzadeh, Z. Sun for help during beam time at the Swiss Light Source. H.V.S., C.M. and S.V.P. thank the Swiss National Science Foundation for the financial support.

Author contributions

H.V.S., S.V.P. designed research, C.M., S.V.P., C.B. performed experiment, C.M., H.V.S., S.V.P. analyzed data and wrote the manuscript.

Additional information

Competing financial interests: The authors declare no competing financial interests.

How to cite this article: Marichal, C., Van Swygenhoven, H., Van Petegem, S. & Borca, C. {110} Slip with {112} slip traces in bcc Tungsten. *Sci. Rep.* **3**, 2547; DOI:10.1038/srep02547 (2013).

This work is licensed under a Creative Commons Attribution-NonCommercial-ShareAlike 3.0 Unported license. To view a copy of this license, visit http://creativecommons.org/licenses/by-nc-sa/3.0